



CHORUS

This is the accepted manuscript made available via CHORUS. The article has been published as:

Electron and Ion Dynamics of the Solar Wind Interaction with a Weakly Outgassing Comet

Jan Deca, Andrey Divin, Pierre Henri, Anders Eriksson, Stefano Markidis, Vyacheslav Olshevsky, and Mihály Horányi

Phys. Rev. Lett. **118**, 205101 — Published 15 May 2017

DOI: [10.1103/PhysRevLett.118.205101](https://doi.org/10.1103/PhysRevLett.118.205101)

Electron and Ion Dynamics of the Solar Wind Interaction with a Weakly Outgassing Comet

Jan Deca,^{1,2,*} Andrey Divin,^{3,4} Pierre Henri,⁵ Anders Eriksson,⁴
Stefano Markidis,⁶ Vyacheslav Olshevsky,⁷ and Mihály Horányi^{1,2}

¹Laboratory for Atmospheric and Space Physics (LASP), University of Colorado Boulder, USA

²Institute for Modeling Plasma, Atmospheres and Cosmic Dust, NASA/SSERVI, USA

³St. Petersburg State University, St. Petersburg, Russia

⁴Swedish Institute of Space Physics (IRF), Uppsala, Sweden

⁵LPC2E, CNRS, Orléans, France

⁶KTH Royal Institute of Technology, Stockholm, Sweden

⁷Centre for mathematical Plasma Astrophysics (CmPA), KU Leuven, leuven, Belgium

Using a 3-D fully kinetic approach, we disentangle and explain the ion and electron dynamics of the solar wind interaction with a weakly outgassing comet. We show that, to first order, the dynamical interaction is representative of a four-fluid coupled system. We self-consistently simulate and identify the origin of the warm and suprathermal electron distributions observed by ESA’s Rosetta mission to comet 67P/Churyumov-Gerasimenko and conclude that a detailed kinetic treatment of the electron dynamics is critical to fully capture the complex physics of mass-loading plasmas.

1 Cometary nuclei are small, irregularly-shaped “icy dirt 36
2 balls,” leftover from the dawn of our Solar System 4.6 37
3 billion years ago, and composed of a mixture of ices, 38
4 refractory materials, and large organic molecules [1–4]. 39
5 When a comet is sufficiently close to the Sun, the 40
6 sublimation of ice leads to an outgassing atmosphere 41
7 and the formation of a coma, and a dust and plasma tail. 42
8 Historically, this process revealed the existence of the 43
9 solar wind and the interplanetary magnetic field [5–8]. 44
10 Comets are critical to decipher the physics of gas release 45
11 processes in space. The latter result in mass-loaded 46
12 plasmas [9, 10], which more than three decades after the 47
13 AMPTE space release experiments [11] are still not fully 48
14 understood. 49

15
16 First observed in 1969, comet 67P/Churyumov- 51
17 Gerasimenko was escorted for almost two years along 52
18 its 6.45yr elliptical orbit by ESA’s Rosetta orbiter 53
19 spacecraft. During the mission, the comet transitioned 54
20 from its weakly outgassing phase into a more active 55
21 object as it approached the Sun, and back again to 56
22 quieter phases when traveling outward in the Solar 57
23 System. This first ever mission to do more than a simple 58
24 cometary fly-by revealed in unprecedented detail the 59
25 fascinating evolution of a comet [12] and the building up 60
26 of its induced magnetosphere [13]. 61

27
28 Up to date, the focus of modelling studies to predict 62
29 and explain the complex cometary plasma observations 63
30 has been on MHD/multi-fluid [14–19] and hybrid (using 64
31 a kinetic description for the ions but describing the 65
32 electrons as a mass-less fluid) [20–26] simulations, 66
33 leading to comprehensive models for the ion dynamics. 67
34 A satisfactory explanation for the observed electron 68
35 dynamics, however, is not yet available. For instance, 69
70

the Ion and Electron Sensor instrument onboard the
Rosetta orbiter shows the presence of non-thermal elec-
tron distributions inside the inhomogeneous expanding
cometary ionosphere, including both a warm (~ 5 eV)
and suprathermal (10-20 eV) component [27–29]. The
origin and physical mechanism behind the various
components of the observed electron distributions is
unclear, but must be understood to disentangle the
cometary plasma dynamics.

We develop and analyse a detailed model of the
cometary plasma dynamics, including fine-scale electron
kinetic physics, and discuss the relative acceleration
mechanisms decoupling the plasma populations. Using
the collisionless semi-implicit, fully kinetic, electromag-
netic particle-in-cell code iPic3D [30], which solves the
Vlasov-Maxwell system of equations for both ions and
electrons using the implicit moment method [31–33], we
focus on the interaction between the solar wind and a
weakly outgassing comet such as encountered by Rosetta
at approximately 3 AU from the Sun. At such large
distances from the Sun, the collisionless approximation is
valid everywhere except in the innermost coma [34, 35].
We model self-consistently the kinetic dynamics of both
cometary water ions and electrons, produced by the
ionisation of the radially expanding and outgassing
cometary atmosphere, together with the incoming solar
wind proton and electron plasma flow. To accommodate
a flowing plasma in the computational domain we use
open boundary conditions as implemented in Deca *et al.*
[36].

Maxwellian distributions of solar wind protons and
electrons are injected at the inflow boundary of the
computational domain (at $x = -1540$ km) with densities
 $n_{p,sw} = n_{e,sw} = 1 \text{ cm}^{-3}$ and temperatures $T_{p,sw} = 7$ eV,
 $T_{e,sw} = 10$ eV, respectively, approximating the free-
streaming solar wind plasma distributions [29, 37]. The
73

* [mailto: jan.deca@gmail.com](mailto:jan.deca@gmail.com)

FIG. 1. Density profiles in the XY/XZ-planes for the solar wind (left panels) and cometary (right panels) ions and electrons. The Y-axis is directed along the solar wind magnetic field. Field lines are plotted in black. The red arrow on panel (c) indicates the deflected solar wind proton flow in the XZ-plane.

74 solar wind flows along X at $\mathbf{v}_{sw} = (400, 0, 0) \text{ km s}^{-1}$.¹⁰⁸
 75 We use a reduced mass-ratio $m_{p,sw}/m_{e,sw} = 100$ to¹⁰⁹
 76 meet our numerical restrictions, a common practice¹¹⁰
 77 in fully kinetic simulations that ensures scale sepa-¹¹¹
 78 ration between electron and ion dynamics [38]. The¹¹²
 79 interplanetary magnetic field is directed along Y at¹¹³
 80 $\mathbf{B}_{IMF} = (0, 6, 0) \text{ nT}$, resulting in a solar wind proton¹¹⁴
 81 and electron Larmor radius of $r_{p,sw} = 142 \text{ km}$ and¹¹⁵
 82 $r_{e,sw} = 12 \text{ km}$, respectively. The nucleus of the comet¹¹⁶
 83 is represented by an absorbing sphere placed 110 km¹¹⁷
 84 upstream of the centre of the computational domain (at¹¹⁸
 85 $(x, y, z) = (-110, 0, 0) \text{ km}$). The computational domain¹¹⁹
 86 measures $3300 \times 2200 \times 2200 \text{ km}^3$ with a resolution of¹²⁰
 87 10 km in all three Cartesian directions. The simulation¹²¹
 88 time step is $\Delta t = 4.5 \cdot 10^{-5} \text{ s}$, which is well below¹²²
 89 the electron gyro-period (5.95 ms for 6 nT) and hence¹²³
 90 resolves the electron gyro-motion.¹²⁴

91
 92 The solar wind is mass-loaded by cold cometary ions¹²⁶
 93 as a consequence of the outgassing cometary neutral¹²⁷
 94 atmosphere that is ionised as it expands [39]. In order to¹²⁸
 95 inject cometary ion/electron pairs, we do not implement¹²⁹
 96 the neutral gas distribution. Instead, we use an analyt-¹³⁰
 97 ical profile for the plasma production rate that results¹³¹
 98 from the ionisation of an expanding neutral gas with a¹³²
 99 $1/r^2$ radial density profile. We assume a gas production¹³³
 100 rate of $Q = 10^{26} \text{ s}^{-1}$ [40]. The resulting cometary¹³⁴
 101 density profile then mimics the $1/r$ plasma density¹³⁵
 102 profile observed close to the cometary nucleus [41]. We¹³⁶
 103 radially inject Maxwell-distributed cometary electrons¹³⁷
 104 ($T_{e,c} = 10 \text{ eV}$) and cold cometary water group ions¹³⁸
 105 ($m_{i,c}/m_{p,sw} = 20$) accordingly. The thermal velocity of¹³⁹
 106 the implanted water ions is set two orders of magnitude¹⁴⁰
 107 smaller than the solar wind protons, which translates in¹⁴¹

a cometary ion temperature of $T_{i,c} = 0.5 \text{ eV}$. Although $T_{i,c}$ is somewhat higher than observed by Rosetta (e.g., Nilsson *et al.* [13]), cometary ions are born in the simulation with energies two-thousand times less than the solar wind energy, ensuring sufficient separation of scales.

Figure 1 shows the density profiles in the XY- (terminator) and XZ- (cross magnetic field) planes for the solar wind (panels a-d) and cometary (panels e-h) ion and electron species. The simulated global structure of the solar wind – weak comet interaction confirms the results reported by hybrid simulations on the induced cometary magnetosphere [23–25]. In particular, we observe a magnetic pileup (a direct consequence of the ionisation of outflowing gas from the nucleus) up to more than three times the interplanetary magnetic field magnitude [42], together with a compression of the incoming, mass-loaded, solar wind (panel a). The magnetic field lines drape around the nucleus. No bow shock develops, as expected for a weakly outgassing comet [22]. The heavy cometary ions are accelerated by the convective electric field, to be eventually picked up far downstream, whereas solar wind protons deflect in the opposite direction in accordance with momentum conservation. Downstream of the nucleus, panels (d) and (g) show a fan-like structure [15] and density fluctuations/filamentation [43] that can be associated with the so-called “singing comet” waves [25].

Focusing on the electron dynamics next (figure 1, panels b, d, f and h), we find that, to first order, the electrons behave as two separate fluids: a solar wind and a cometary electron fluid. We observe a spatial separation

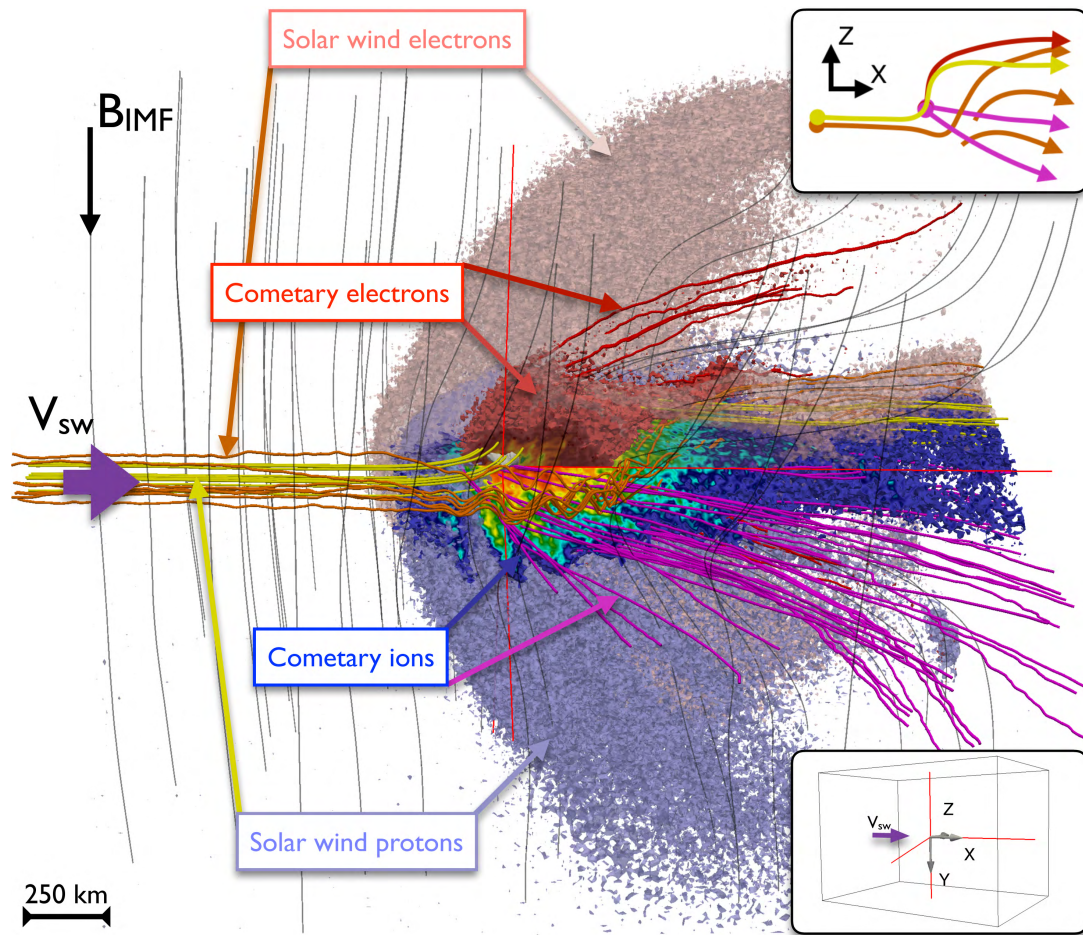


FIG. 2. 3-D overview of the four-fluid behaviour of the solar wind interaction with a weakly outgassing comet. Included in the illustration are the structure of the interplanetary magnetic field, density thresholds and velocity streamlines for the four simulated species. The shape model of 67P-Churyumov-Gerasimenko is five times enlarged to increase visibility. The lower right inset indicates how the density thresholds are cut. The upper right inset illustrates the decoupling of the four species in the XZ-plane, perpendicular to the interplanetary magnetic field.

142 of the cometary electrons with respect to the cometary
 143 ions, and of the solar wind electrons with respect to the
 144 solar wind protons. Cometary electrons eventually end
 145 up neutralising the solar wind protons, and solar wind
 146 electrons eventually neutralise the cometary ions.
 147

148 The four species interact as follows. First, as cometary
 149 ions accelerate along the convective electric field in
 150 the cross magnetic field direction, cometary electrons
 151 are initially accelerated in the opposite direction.
 152 They are picked-up into the solar wind flow much
 153 faster than the cometary ions, at scales larger than
 154 the electron gyro-radius (~ 10 km). In other words,
 155 cometary electrons reach the solar wind flow velocity
 156 very locally (quickly) as compared to the cometary
 157 ions. This process spatially separates the cometary ion
 158 and electron dynamics. Second, this separation of the
 159 ion and electron motion results in a net current that
 160 is associated to a Hall electric field. Coupled to the
 161 need for quasi-neutrality at those scales, the solar wind

electrons become decoupled from the solar wind protons
 upstream of the comet. At the same time, the convective
 electric field has an opposite sign in the solar wind and
 cometary ion reference frame and transfers momentum
 between the two species. While the solar wind protons
 are deflected, the interplanetary magnetic field continues
 to be carried close to the comet through the solar wind
 (and cometary) electrons as they are still frozen-in into
 the magnetic field. This behaviour is quite similar to
 the ion diffusion region in magnetic reconnection [44].

From a kinetic point of view, the simulated four-fluid
 interaction, in particular the separation of the solar wind
 and cometary electron dynamics, is coherent. Solar wind
 and cometary electrons populate different regions in
 phase space when close to the comet. They can therefore
 follow different phase-space trajectories. The velocity
 streamlines shown in Figure 2 illustrate the four-fluid
 behaviour.

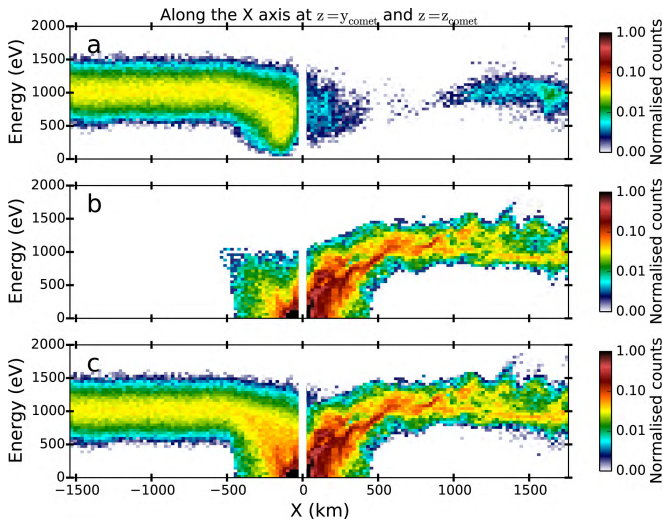


FIG. 3. Solar wind, cometary and total (solar wind + cometary) ion energy distributions along the Sun-comet direction (panel a→c, respectively). The cut is indicated on panel (a) of figure 1. The white band represents the comet location.

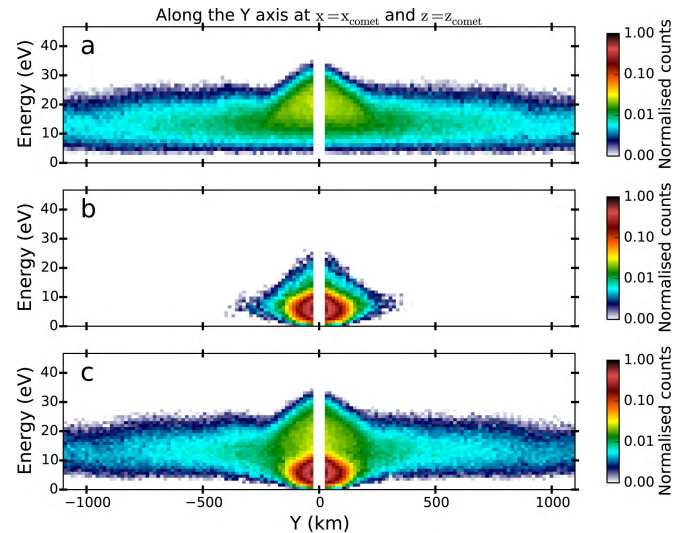


FIG. 4. Solar wind, cometary and total (solar wind + cometary) electron energy distributions along a cut in the terminator plane (panel a→c, respectively). The cut is indicated on panel (e) of figure 1. The white band represents the comet location.

182 The ability of our model to self-consistently describe
 183 the electron-kinetic dynamics of the solar wind - comet
 184 interaction shines a new light on the (observed) particle
 185 energy distributions [29, 45]. Figure 3 shows the solar
 186 wind, cometary, and total ion energy distributions along
 187 the Sun-comet direction (through the centre of the
 188 computational domain, the cut is indicated on panel
 189 (a) of figure 1). The distributions are constructed by
 190 grouping the particle energies in uniform bins, collecting
 191 all particles per species available in $30 \times 30 \times 30 \text{ km}^3$ cubic
 192 domains along the X-direction. Figure 4 is constructed
 193 similarly, but along the Y-axis of the domain.

194
 195 Close to the cometary nucleus, no stagnation point is
 196 observed. Instead, the solar wind proton distribution
 197 loses part of its energy (Figure 3, panel a) as the
 198 incoming plasma is deflected when interacting with the
 199 cometary coma. The lost energy is transferred to the
 200 cometary ions that are picked up by the local convective
 201 electric field and accelerated tail-ward (panel b). This
 202 is qualitatively consistent with the observed energy
 203 behaviour of the solar wind ions [46].

204
 205 The cometary ion energy rises to 1000 eV in the solar
 206 wind proton wake behind the comet, a number compara-
 207 ble to the upstream solar wind proton energy (Figure 3,
 208 panel c). Moving downstream and along the positive
 209 Z-axis (not shown), however, we gradually encounter
 210 more energetic cometary ions as they are being picked
 211 up. At the edge of our computational domain the
 212 cometary ion population has already reached energies
 213 of 1750 eV. Eventually, far beyond our computational
 214 domain [15], the velocity of the cometary ion population
 215 will equal the solar wind flow velocity ($T_{i,c} \rightarrow 20\,000 \text{ eV}$

given our cometary ion mass ratio, $m_{i,c}/m_{p,sw} = 20$).

We measure deflection angles in excess of 45° for both the solar wind protons and cometary ions. In addition, at a fixed location in space with respect to the comet, the pick-up angle is larger for cometary ions with greater energies [47]. Both observations are in agreement with recent plasma measurements by the Rosetta spacecraft [48, 49].

Figure 4 shows the solar wind, cometary, and total electron energy distributions along a cut in the terminator plane (where Rosetta has resided most of the time, the cut is indicated on panel (e) of Figure 1). Solar wind electrons accelerate towards the comet (panel a) under influence of an ambipolar electric field that is generated by the large electron pressure gradient in the inhomogeneous cometary plasma [50], which further enhances the separation of the solar wind electron and ion flows. The total electron energy distribution (panel c) is once again the sum of panels (a) and (b). Close to the comet we observe a warm $\sim 5 \text{ eV}$ component of cometary origin and a $10 - 20 \text{ eV}$ suprathermal component of solar wind origin. Our simulation self-consistently generates both components and reveals the origin of the two collisionless electron distributions observed by Rosetta in the cometary environment [27–29, 45]. Note that a third, cold electron population has also been observed much closer to the Sun, when the electron-neutral collision rate, still negligible at 3 A.U., becomes high enough to cool down the warm cometary electrons [51].

Identifying the origin of the suprathermal electron pop-

ulation delivers clues to the physical mechanism behind their acceleration/heating in the collisionless coma. Two mechanisms have been discussed in literature thus far: (i) heating of electrons through wave-particle interactions such as the “singing comet waves” (understood as an Weibel instability [43, 52]) or lower hybrid waves [45] and (ii) the acceleration of electrons along the ambipolar electric field [29]. In the second scenario, solar wind electrons traveling toward the comet fall into the potential well that is generated by the gradient in electron number density [53, 54]. Electrons born inside, i.e., the cometary electrons, are trapped unless they carry enough energy to escape. The potential scales as the electron thermal energy [29], hence, only suprathermal electrons will be able to escape the near-comet environment. Note that this interpretation is valid on sub-ion time scales only, as quasi-neutrality will act such that electrons must eventually leave the potential well. Without ruling out the influence of wave-particle interactions, our simulation favours the ambipolar electric field model, though this may not be the case at other activity phases of the comet.

We have focused here on a weakly-outgassing cometary nucleus, where the plasma can be safely approximated as collisionless. We use the collisionopause or exobase distance, defined as the distance to the nucleus where the cometocentric distance equals the mean free path for collisions with neutrals, to characterise the validity of this assumption. For $Q = 10^{26} \text{ s}^{-1}$, we find the ion exobase at 3 km above the surface of the nucleus [35, 51]. The electrons are collisionless down to the nucleus. Note that the ion value is computed here for very low energy ions, relevant for newborn ions inheriting the $\sim 200\text{K}$ temperature of the neutral gas. As the ion-neutral cross section rapidly decreases with energy, even a weak electric field combined with a high gas production rate may significantly decrease the ion collisionality [55]. Hence, while there may be some collisionality also in our case, we expect this to be the case only within the first few kilometres above the nucleus (not resolved in our simulation).

As the cometary outgassing activity increases, plasma-neutral collisions will play an increasingly significant role in shaping the ionised cometary environment. Collisions account for two significant processes in the context of mass-loaded plasmas: ion-neutral friction and electron cooling. When the gas production rate is high enough, plasma-neutral collisions eventually carve out a non-magnetised region near the cometary nucleus [56]. This region is shaped by electron-neutral collisions [57]. Taking into account collisions will be necessary to extend this study for more active comets.

To conclude, we have produced the first 3-D fully kinetic and electromagnetic simulations of the solar wind interaction with a weakly outgassing comet, for

which the collisional interaction between the neutral gas and (mass-loading) plasma can be ignored, as is representative of comet 67P/Churyumov-Gerasimenko at 3 AU. We have disentangled the collisionless electron- and ion-kinetic activity of the interaction and found that the electron dynamics, to first order, is that of two independent electron fluids. This allows us to interpret the main features and origin of the warm (cometary) and suprathermal (solar wind) electron distributions observed by the Rosetta mission. Although globally the dynamics of the solar wind – weak comet system is that of a four-fluid coupled system, we conclude that a multi-species electron-kinetic description is a must to fully capture the complex global solar wind – comet interaction process.

This work was supported in part by NASA’s Solar System Exploration Research Virtual Institute (SSERVI): Institute for Modeling Plasmas, Atmosphere, and Cosmic Dust (IMPACT), and the NASA High-End Computing (HEC) Program through the NASA Advanced Supercomputing (NAS) Division at Ames Research Center. Part of this work was inspired by discussions within International Team 336: “Plasma Surface Interactions with Airless Bodies in Space and the Laboratory” at the International Space Science Institute, Bern, Switzerland. Work at LPC2E/CNRS was supported by CNES and by ANR under the financial agreement ANR-15-CE31-0009-01. Partial support is also acknowledged by the contract JPL-1502225 at the University of Colorado from Rosetta, which is an ESA mission with contributions from its member states and NASA.

-
- [1] F. L. Whipple, *Astrophysical Journal* **111**, 375 (1950).
 - [2] H. U. Keller, in *Physics and Mechanics of Cometary Materials*, ESA Special Publication, Vol. 302, edited by J. J. Hunt and T. D. Guyenne (1989).
 - [3] W. M. Irvine, F. P. Schloerb, J. Crovisier, B. Fegley, Jr., and M. J. Mumma, *Protostars and Planets IV*, 1159 (2000).
 - [4] J. M. Sunshine, M. F. A’Hearn, O. Groussin, J.-Y. Li, M. J. S. Belton, W. A. Delamere, J. Kissel, K. P. Klaasen, L. A. McFadden, K. J. Meech, H. J. Melosh, P. H. Schultz, P. C. Thomas, J. Veverka, D. K. Yeomans, I. C. Busko, M. Desnoyer, T. L. Farnham, L. M. Feaga, D. L. Hampton, D. J. Lindler, C. M. Lisse, and D. D. Wellnitz, *Science* **311**, 1453 (2006).
 - [5] L. Biermann, *Zeitschrift für Astrophysik* **29**, 274 (1951).
 - [6] H. Alfvén, *Tellus* **9** (1957).
 - [7] L. Biermann, B. Brosowski, and H. U. Schmidt, *Solar Physics* **1**, 254 (1967).
 - [8] D. A. Mendis, H. L. F. Houppis, and M. L. Marconi, *Fundamentals of Cosmic Physics* **10**, 2 (1985).
 - [9] K. Szegő, K.-H. Glassmeier, R. Bingham, A. Bogdanov, C. Fischer, G. Haerendel, A. Brinca, T. Cravens, E. Dubinin, K. Sauer, L. Fisk, T. Gombosi, N. Schwadron, P. Isenberg, M. Lee, C. Mazelle, E. Möbius,

- U. Motschmann, V. D. Shapiro, B. Tsurutani, and G. Zank, *Space Science Reviews* **94**, 429 (2000).
- [10] T. I. Gombosi, in *Magnetotails in the Solar System*, Washington DC American Geophysical Union Geophysical Monograph Series, Vol. 207, edited by A. Keiling, C. M. Jackman, and P. A. Delamere (2015) pp. 169–188.
- [11] G. Haerendel, G. Paschmann, W. Baumjohann, and C. W. Carlson, *Nature* **320**, 720 (1986).
- [12] M. G. G. T. Taylor, C. Alexander, N. Altobelli, M. Fulle, M. Fulchignoni, E. Grün, and P. Weissman, *Science* **347**, 387 (2015).
- [13] H. Nilsson, G. Stenberg Wieser, E. Behar, C. S. Wedlund, H. Gunell, M. Yamauchi, R. Lundin, S. Barabash, M. Wieser, C. Carr, E. Cupido, J. L. Burch, A. Fedorov, J.-A. Sauvaud, H. Koskinen, E. Kallio, J.-P. Lebreton, A. Eriksson, N. Edberg, R. Goldstein, P. Henri, C. Koenders, P. Mokashi, Z. Nemeth, I. Richter, K. Szego, M. Volwerk, C. Vallat, and M. Rubin, *Science* **347**, aaa0571 (2015).
- [14] Y. D. Jia, M. R. Combi, K. C. Hansen, T. I. Gombosi, F. J. Crary, and D. T. Young, *Icarus* **196**, 249 (2008).
- [15] M. Rubin, C. Koenders, K. Altwegg, M. R. Combi, K.-H. Glassmeier, T. I. Gombosi, K. C. Hansen, U. Motschmann, I. Richter, V. M. Tennishev, and G. Tóth, *Icarus* **242**, 38 (2014).
- [16] M. Rubin, M. R. Combi, L. K. S. Daldorff, T. I. Gombosi, K. C. Hansen, Y. Shou, V. M. Tennishev, G. Tóth, B. van der Holst, and K. Altwegg, *The Astrophysical Journal* **781**, 86 (2014).
- [17] M. Rubin, T. I. Gombosi, K. C. Hansen, W.-H. Ip, M. D. Kartalev, C. Koenders, and G. Tóth, *Earth Moon and Planets* **116**, 141 (2015).
- [18] Z. Huang, G. Tóth, T. I. Gombosi, X. Jia, M. Rubin, N. Fougere, V. Tennishev, M. R. Combi, A. Bieler, K. C. Hansen, Y. Shou, and K. Altwegg, *Journal of Geophysical Research (Space Physics)* **121**, 4247 (2016).
- [19] Y. Shou, M. Combi, G. Toth, V. Tennishev, N. Fougere, X. Jia, M. Rubin, Z. Huang, K. Hansen, T. Gombosi, and A. Bieler, *The Astrophysical Journal* **833**, 160 (2016).
- [20] N. Gortsas, U. Motschmann, E. Kührt, J. Knollenberg, S. Simon, and A. Boesswetter, *Annales Geophysicae* **27**, 1555 (2009).
- [21] S. Wiehle, U. Motschmann, N. Gortsas, K.-H. Glassmeier, J. Müller, and C. Koenders, *Advances in Space Research* **48**, 1108 (2011).
- [22] C. Koenders, K.-H. Glassmeier, I. Richter, U. Motschmann, and M. Rubin, *Planetary and Space Science* **87**, 85 (2013).
- [23] C. Koenders, K.-H. Glassmeier, I. Richter, H. Ranocha, and U. Motschmann, *Planetary and Space Science* **105**, 101 (2015).
- [24] E. Behar, J. Lindkvist, H. Nilsson, M. Holmström, G. Stenberg-Wieser, R. Ramstad, and C. Götz, *Astronomy & Astrophysics* **596**, A42 (2016).
- [25] C. Koenders, C. Goetz, I. Richter, U. Motschmann, and K.-H. Glassmeier, *Monthly Notices of the Royal Astronomical Society* **462**, S235 (2016).
- [26] C. Koenders, C. Perschke, C. Goetz, I. Richter, U. Motschmann, and K. H. Glassmeier, *Astronomy & Astrophysics* **594**, A66 (2016).
- [27] G. Clark, T. W. Broiles, J. L. Burch, G. A. Collinson, T. Cravens, R. A. Frahm, J. Goldstein, R. Goldstein, K. Mandt, P. Mokashi, M. Samara, and C. J. Pollock, *Astronomy & Astrophysics* **583**, A24 (2015).
- [28] T. W. Broiles, G. Livadiotis, J. L. Burch, K. Chae, G. Clark, T. E. Cravens, R. Davidson, A. Eriksson, R. A. Frahm, S. A. Fuselier, J. Goldstein, R. Goldstein, P. Henri, H. Madanian, K. Mandt, P. Mokashi, C. Pollock, A. Rahmati, M. Samara, and S. J. Schwartz, *Journal of Geophysical Research (Space Physics)* **121**, 7407 (2016).
- [29] H. Madanian, T. E. Cravens, A. Rahmati, R. Goldstein, J. Burch, A. I. Eriksson, N. J. T. Edberg, P. Henri, K. Mandt, G. Clark, M. Rubin, T. Broiles, and N. L. Reedy, *Journal of Geophysical Research (Space Physics)* **121**, 5815 (2016).
- [30] S. Markidis, G. Lapenta, and Rizwan-uddin, *Mathematics and Computers in Simulation* **80**, 1509 (2010).
- [31] R. J. Mason, *Journal of Computational Physics* **41**, 233 (1981).
- [32] J. U. Brackbill and D. W. Forslund, *Journal of Computational Physics* **46**, 271 (1982).
- [33] G. Lapenta, J. U. Brackbill, and P. Ricci, *Physics of Plasmas* **13**, 055904 (2006).
- [34] T. E. Cravens, Washington DC American Geophysical Union Geophysical Monograph Series **61**, 27 (1991).
- [35] K. E. Mandt, A. Eriksson, N. J. T. Edberg, C. Koenders, T. Broiles, S. A. Fuselier, P. Henri, Z. Nemeth, M. Alho, N. Biver, A. Beth, J. Burch, C. Carr, K. Chae, A. J. Coates, E. Cupido, M. Galand, K.-H. Glassmeier, C. Goetz, R. Goldstein, K. C. Hansen, J. Haiducek, E. Kallio, J.-P. Lebreton, A. Luspay-Kuti, P. Mokashi, H. Nilsson, A. Opitz, I. Richter, M. Samara, K. Szego, C.-Y. Tzou, M. Volwerk, C. Simon Wedlund, and G. Stenberg Wieser, *Monthly Notices of the Royal Astronomical Society* **462**, S9 (2016).
- [36] J. Deca, A. Divin, B. Lembège, M. Horányi, S. Markidis, and G. Lapenta, *Journal of Geophysical Research: Space Physics*, 6443 (2015), 2015JA021070.
- [37] K. C. Hansen, T. Bagdonat, U. Motschmann, C. Alexander, M. R. Combi, T. E. Cravens, T. I. Gombosi, Y.-D. Jia, and I. P. Robertson, *Space Science Reviews* **128**, 133 (2007).
- [38] A. Bret and M. E. Dieckmann, *Physics of Plasmas* **17**, 032109 (2010).
- [39] T. I. Gombosi, M. Horanyi, K. Kecskemety, T. E. Cravens, and A. F. Nagy, *Astrophysical Journal* **268**, 889 (1983).
- [40] A. Bieler, K. Altwegg, H. Balsiger, J.-J. Berthelier, U. Calmonte, M. Combi, J. De Keyser, B. Fiethe, N. Fougere, S. Fuselier, S. Gasc, T. Gombosi, K. Hansen, M. Hässig, Z. Huang, A. Jäckel, X. Jia, L. Le Roy, U. A. Mall, H. Rème, M. Rubin, V. Tennishev, G. Tóth, C.-Y. Tzou, and P. Wurz, *Astronomy & Astrophysics* **583**, A7 (2015).
- [41] N. J. T. Edberg, A. I. Eriksson, E. Odelstad, P. Henri, J.-P. Lebreton, S. Gasc, M. Rubin, M. André, R. Gill, E. P. G. Johansson, F. Johansson, E. Vigren, J. E. Wahlund, C. M. Carr, E. Cupido, K.-H. Glassmeier, R. Goldstein, C. Koenders, K. Mandt, Z. Nemeth, H. Nilsson, I. Richter, G. S. Wieser, K. Szego, and M. Volwerk, *Geophysical Research Letters* **42**, 4263 (2015).
- [42] M. Volwerk, I. Richter, B. Tsurutani, C. Götz, K. Altwegg, T. Broiles, J. Burch, C. Carr, E. Cupido, M. Delva, M. Dósa, N. J. T. Edberg, A. Eriksson, P. Henri, C. Koenders, J.-P. Lebreton, K. E. Mandt, H. Nilsson, A. Opitz, M. Rubin, K. Schwingenschuh, G. Stenberg Wieser, K. Szegö, C. Vallat, X. Vallieres,

- and K.-H. Glassmeier, *Annales Geophysicae* **34**, 1 (2016).
- [43] I. Richter, C. Koenders, H.-U. Auster, D. Frühauff, C. Götz, P. Heinisch, C. Perschke, U. Motschmann, B. Stoll, K. Altwegg, J. Burch, C. Carr, E. Cupido, A. Eriksson, P. Henri, R. Goldstein, J.-P. Lebreton, P. Mokashi, Z. Nemeth, H. Nilsson, M. Rubin, K. Szegő, B. T. Tsurutani, C. Vallat, M. Volwerk, and K.-H. Glassmeier, *Annales Geophysicae* **33**, 1031 (2015).
- [44] B. U. Ö. Sonnerup, “Magnetic field reconnection,” in *Solar System Plasma Physics*, edited by L. J. Lanzerotti, C. F. Kennel, and E. N. Parker (North-Holland Publishing Co., 1979) pp. 45–108.
- [45] T. W. Broiles, J. Burch, K. Chae, G. Clark, T. Cravens, A. Eriksson, S. Fuselier, R. Frahm, S. Gasc, R. Goldstein, P. Henri, C. Koenders, G. Livadiotis, K. Mandt, P. Mokashi, Z. Nemeth, E. Odelstad, M. Rubin, and M. Samara, *Monthly Notices of the Royal Astronomical Society* (2016), 10.1093/mnras/stw2942.
- [46] H. Nilsson, G. Stenberg Wieser, E. Behar, C. S. Wedlund, E. Kallio, H. Gunell, N. J. T. Edberg, A. I. Eriksson, M. Yamauchi, C. Koenders, M. Wieser, R. Lundin, S. Barabash, K. Mandt, J. L. Burch, R. Goldstein, P. Mokashi, C. Carr, E. Cupido, P. T. Fox, K. Szego, Z. Nemeth, A. Fedorov, J.-A. Sauvaud, H. Koskinen, I. Richter, J.-P. Lebreton, P. Henri, M. Volwerk, C. Vallat, and B. Geiger, *Astronomy & Astrophysics* **583**, A20 (2015).
- [47] A. Divin, J. Deca, P. Henri, A. Eriksson, S. Markidis, and M. Horányi, in *AGU Fall meeting*, AGU Fall meeting, Vol. 0 (2016) p. 0.
- [48] T. W. Broiles, J. L. Burch, G. Clark, C. Koenders, E. Behar, R. Goldstein, S. A. Fuselier, K. E. Mandt, P. Mokashi, and M. Samara, *Astronomy & Astrophysics* **583**, A21 (2015).
- [49] E. Behar, H. Nilsson, G. S. Wieser, Z. Nemeth, T. W. Broiles, and I. Richter, *Geophysical Research Letters* **43**, 1411 (2016).
- [50] A. Divin, J. Deca, P. Henri, A. Eriksson, S. Markidis, and M. Horányi, *Monthly Notices of the Royal Astronomical Society* **0**, 0 (2017).
- [51] A. I. Eriksson, I. A. D. Engelhardt, M. A. R. Boström, N. J. T. Edberg, F. L. Johansson, E. Odelstad, E. Vigren, J.-E. Wahlund, P. Henri, J.-P. Lebreton, W. J. Miloch, J. J. P. Paulsson, C. S. Wedlund, L. Yang, T. Karlsson, R. Jarvinen, T. Broiles, K. Mandt, C. M. Carr, M. Galand, H. Nilsson, and C. Norberg, *Astronomy&Astrophysics* **accepted for publication** (2017).
- [52] P. Meier, K.-H. Glassmeier, and U. Motschmann, *Annales Geophysicae* **34**, 691 (2016).
- [53] E. Vigren, M. Galand, A. I. Eriksson, N. J. T. Edberg, E. Odelstad, and S. J. Schwartz, *Astrophysical Journal* **812**, 54 (2015).
- [54] T. E. Cravens, T. I. Gombosi, B. E. Gribov, M. Horanyi, K. Kecskemety, A. Korosmezey, M. L. Marconi, D. A. Mendis, A. F. Nagy, R. Z. Sagdeev, V. I. Shevchenko, V. D. Shapiro, and K. Szego, *Role of electric fields in the cometary environment*. (Hungarian Acad. Sci., 1984).
- [55] E. Vigren and A. I. Eriksson, *The Astronomical Journal* **153**, 150 (2017).
- [56] C. Goetz, C. Koenders, I. Richter, K. Altwegg, J. Burch, C. Carr, E. Cupido, A. Eriksson, C. Güttler, P. Henri, P. Mokashi, Z. Nemeth, H. Nilsson, M. Rubin, H. Sierks, B. Tsurutani, C. Vallat, M. Volwerk, and K.-H. Glassmeier, *Astronomy & Astrophysics* **588**, A24 (2016).
- [57] P. Henri, X. Vallières, C. Goetz, I. Richter, K.-H. Glassmeier, M. Galand, M. Rubin, A. Eriksson, Z. Nemeth, E. Vigren, A. Beth, J. Burch, C. Carr, H. Nilsson, B. Tsurutani, and G. Wattieaux, *Monthly Notices of the Royal Astronomical Society* **submitted** (2017).